All-Optical Pulse Reshaping and Retiming Systems Incorporating Pulse Shaping Fiber Bragg Grating

Francesca Parmigiani, Periklis Petropoulos, Morten Ibsen, and David J. Richardson

***Abstract*—This paper demonstrates two optical pulse retiming and reshaping systems incorporating superstructured fiber Bragg gratings (SSFBGs) as pulse shaping elements. A rectangular switching window is implemented to avoid conversion of the timing jitter on the original data pulses into pulse amplitude noise at the output of a nonlinear optical switch. In a first configuration, the rectangular pulse generator is used at the (low power) data input to a nonlinear optical loop mirror (NOLM) to perform retiming of an incident noisy data signal using a clean local clock signal to control the switch. In a second configuration, the authors further amplify the data signal and use it to switch a (low power) clean local clock signal. The S-shaped nonlinear characteristic of the NOLM results in this instance in a reduction of both timing and amplitude jitter on the data signal. The underlying technologies required for the implementation of this technique are such that an upgrade of the scheme for the regeneration of ultrahigh bit rate signals at data rates in excess of 320 Gb/s should be achievable.**

***Index Terms*—All-optical regeneration, fiber Bragg grating, nonlinear optical loop mirror, optical pulse shaping, ultrashort optical pulses.**

I. Introduction

FIBER Bragg gratings (FBGs) are commonly used in telecommunication systems for familiar applications such as add-drop filtering of dense wavelength division multiplexing (DWDM) channels and dispersion compensation. More recently, a new form of FBG has been developed, the so-called superstructured FBG (SSFBG), which allows the production of designer optical filters with accurately controlled frequency and phase responses of almost arbitrary complexity in a single continuous grating structure [1]–[4]. The fabrication of SSFBGs requires precise control of the refractive index modulation along the grating length. SSFBGs have proven to be an extremely powerful tool for advanced photonic applications that require accurate manipulation of the exact shape of short optical pulses. Pulse shaping with SSFBGs relies upon designing and fabricating a grating with a spectral response such that a preknown spectrum of relatively broadband short pulses will be transformed upon reflection from the structure into a desired spectral form while maintaining the coherent properties of the pulses. This linear technique has a range of attractive features including simple implementation, robust polarization insensitive operation, flexibility, and applicability to various optical communication system functions. Several applications that make use of this technique have successfully been explored to date, ranging from encoding/decoding within coherent optical code division multiple access (OCDMA) systems [2] to pulse repetition rate multiplication [3]. Another interesting application of this linear optical technique relates to the reshaping of short pulses of a few picosecond duration into rectangular pulses [4], [5]—such shaping is difficult to perform by other means. These pulse forms can be very useful for applications that require a rectangular window for nonlinear optical switching such as jitter tolerant optical demultiplexing of short data pulses [6].

In this paper, we demonstrate in a proof-of-principle experiment a technique that uses a combination of a linear rectangular pulse shaping SSFBG and a nonlinear switch for drastically reducing the timing jitter introduced in short pulse transmission systems. In our case, the nonlinear switch is a nonlinear optical loop mirror (NOLM). The technique relies upon reshaping return to zero (RZ)-signal data pulses into relatively long rectangular pulses and then switching these pulses with a synchronous optical clock signal.

In the past, we used similar SSFBG structures to broaden the operating window of optical demultiplexers operating at repetition rates of up to 80 Gb/s, thus significantly relaxing the requirement for precise timing between the data and the control pulses [5], [7]. This previous scheme used (high power) shaped rectangular pulses as the control signal to a nonlinear switch based on an NOLM. However, timing jitter on the original data pulses is not eliminated with this scheme and is passed on directly to the demultiplexed signal. In the present demonstration, we have extended the concept and have applied the shaping function to the data rather than the clock signal incident to the optical switch. This has allowed us not only to have timing-jitter-tolerant operation of the switch but also to retime the data pulses at the switch output.

A similar technique for generating a rectangular switching window at the input of an optical regenerator was developed in [8] in a 160-Gb/s transmission experiment. In that scheme, the pulse shaper was based on obtaining controllable pulse broadening in a Hi–Bi fiber due to polarization mode walk-off. However, the polarization sensitivity of this approach is likely to represent a practical limiting factor for its application within a real system. Also, the width of the rectangular pulse cannot be arbitrarily chosen if a flattened-top signal is desired. In [6], a rectangular switching window was obtained in an NOLM by making use of the walk-off generated between the co propagating control and the signal pulses in the fiber incorporated in the loop. This scheme, however, compromises the efficiency

Manuscript received February 15, 2005; revised September 6, 2005. This work was supported in part by EU-FP6 NoE e-Photon/ONe, WP5, and WP10.

The authors are with the Optoelectronics Research Centre (ORC), University of Southampton, Highfield, Southampton SO17 1BJ, U.K. (e-mail: frp@orc.soton.ac.uk; pp@orc.soton.ac.uk; mi@orc.soton.ac.uk; djr@orc.soton.ac.uk).

Digital Object Identifier 10.1109/JLT.2005.860157

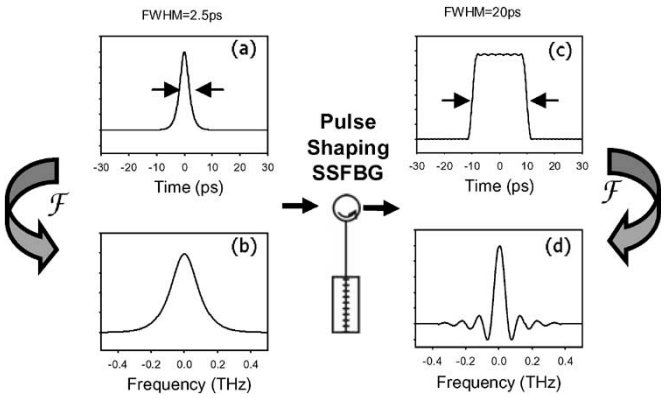

Fig. 1. Simulation graphs of the electric field representation of the (a) and (b) input 2.5-ps soliton pulses and (c) and (d) the output 20-ps square pulses in the time and frequency domain, respectively.

of the switch and makes the operation of the system strongly wavelength dependent.

Fig. 1 shows schematically the design procedure for the pulse shaping SSFBG we have used in our experiments (a detailed analysis can be found in [4]). For our demonstration, we targeted 20-ps rectangular pulses at a repetition rate of 10 GHz [see Fig. 1(c)] starting from 2.5-ps soliton-like data pulses [see Fig. 1(a)]. The initial pulses needed to be filtered via the SSFBG such that the representation of the electric field of the reflected signal in the frequency domain was a sinc-function consisting of alternating lobes of the inverse phase [see Fig. 1(d)]. These pulse parameters were chosen to allow us to perform a detailed assessment of the performance of the system under well-controlled artificially induced signal noise conditions. It should be noted that the SSFBG design can be modified to accommodate different pulse width requirements for application at systems of different repetition rate (see, e.g., [5]).

The basic idea behind the retiming scheme is shown in Fig. 2. The figure schematically shows what is happening in an all-optical switching device in the instance that (a) no retiming or (b) a rectangular-switching-window retiming technique is applied to the signal. As can be seen in case (a), large timing jitter of the signal pulses results in significant pulse amplitude noise at the output of the switch when the signal is switched by a short optical pulse. Our retiming technique, case (b), relies on the incorporation of an intermediate stage within which each data pulse is reshaped into a rectangular pulse prior to being injected into the switch. The maximum tolerable amount of timing jitter that can be suppressed is defined by the duration of the rectangular pulse and cannot be larger than the duration allocated to each data slot. The signal is then switched by clean short clock signal pulses that are temporally aligned to the nominal center of the rectangular data pulses. The clock signal ensures that the output signal is retimed and that it maintains the original pulse width. In this way, even if the switching pulse is very short, the flat-topped signal generated by the SSFBG ensures that the switch is insensitive to any mistiming of the original signal. Note that our reshaping mechanism is reasonably robust and not particularly sensitive to the input pulse shape, wavelength misalignment, and grating imperfections (see [4]). This scheme can be used in conjunction with a common reshaping regenerator with a nonlinear characteristic similar to that of an ideal hard limiter in order to avoid the transfer of any amplitude noise from the original signal to the regenerated signal. It is well known that a suitably biased NOLM has such a nonlinear transfer characteristic and is able to reduce the noise both on the zeros and the marks of the control signal provided that the peak power of the control pulses reaches the value required to achieve $\sim \pi$ nonlinear phase shift over the length of the fiber inside the loop [9]. We will discuss in the later sections of this paper how this can be used for the simultaneous implementation of retiming and reshaping in a single NOLM switch. To simplify our experiments, we did not incorporate a clock recovery into our system as would be required to synchronize the clock and data pulses in any real-world implementation of a regenerator based on our approach. In principle, this is not a major issue, and the development and requirements for a suitable clock recovery circuit is not considered further in this work.

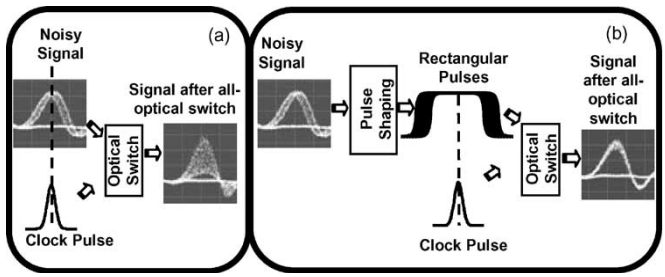

Fig. 2. Principle of the retiming technique as applied to RZ signals. Switching (a) without and (b) with the use of shaped rectangular pulses.

This paper is organized as follows. In Section II, we present an experimental characterization of the rectangular-shaped pulses used in our experiments as performed using a fiberized optical sampling oscilloscope. The performance of our scheme as a pure retimer is assessed in Section III. In Section IV, we modify the configuration of the nonlinear switch, extending the functionality of the system to obtain pulse reshaping/amplitude noise reduction as well as retiming of the data pulses. This is achieved by feeding the shaped data signal onto the control port of the nonlinear switch. The S-shaped switching characteristic of the NOLM combined with the square switching window provides simultaneous pulse reshaping and amplitude noise reduction. We demonstrate the improvement in the noise performance of our system through bit error rate (BER), histogram, and eye diagram measurements.

II. Assessment of the Shaped Pulses

It follows from Fig. 2 that any variation in amplitude across the rectangular-shaped pulses will directly affect the performance of the retiming system—resulting in induced amplitude noise. It was therefore deemed necessary to assess the quality of the rectangular pulses in detail before progressing with our retiming/reshaping experiments. However, because of the ultrafast features of the shaped signal, high-resolution diagnostic tools were needed to accurately measure the precise waveform. A conventional short-pulse measurement provided by a second

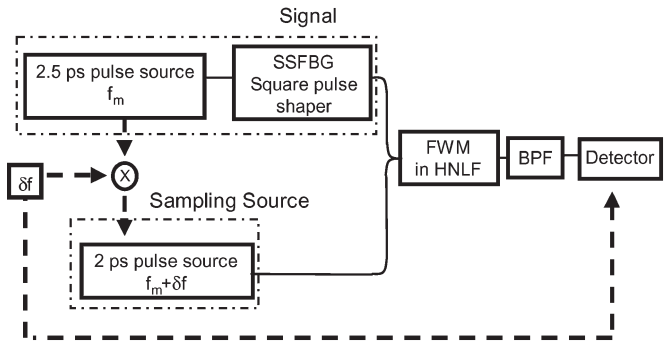

Fig. 3. Block diagram of the optical sampling technique used to assess the 20-ps square pulses (BPF: bandpass filter).

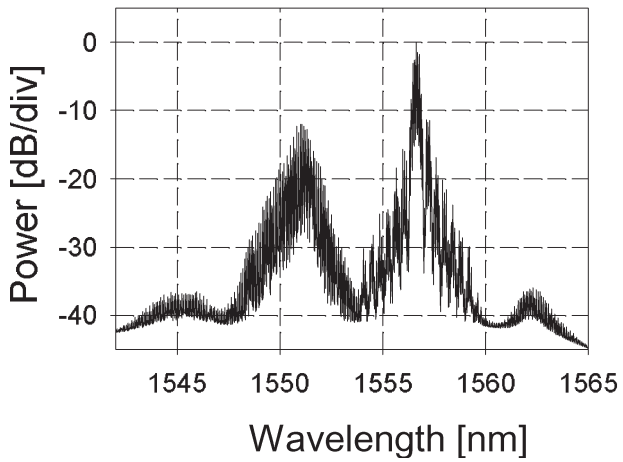

Fig. 4. Optical spectrum after the HNLF. The signal is 20-ps rectangular pulses.

harmonic autocorrelator is not adequate in this case since it can only provide limited and indirect information on the exact shape of the pulses. We therefore opted instead to build and use an optical sampling oscilloscope. This can provide real-time measurements with a relatively high resolution and is well suited to the characterization of pulses shaped by SSFBGs. Fig. 3 shows a block diagram of the optical sampling scope we built [10]. Our sampling signal was generated using four-wave mixing (FWM) in a highly nonlinear fiber (HNLF). By filtering the FWM product, we obtained a signal that was proportional to the intensity of the sampled signal. An example of the spectrum obtained after the nonlinear interaction of the signal with the sampling pulses is given in Fig. 4. Note the sinc-function features of the rectangular signal at a wavelength of $\sim$ 1556.8 nm. The resolution of the measuring setup was 2 ps, limited by the pulse width of the sampling source. Fig. 5 shows the shaped 20-ps rectangular pulses at a repetition rate of 10 GHz measured with the optical sampling scope. The pulses are seen to have sharp trailing and leading edges and a good flat top section. The relative ripple depth at the top, defined as the ratio of the difference between the highest and the lowest intensity points of the ripple, to the maximum pulse intensity is less than 5%. The inset of Fig. 5 shows a second harmonic autocorrelation of the same pulses as expected for rectangular pulses. As noted above, little information about the detailed

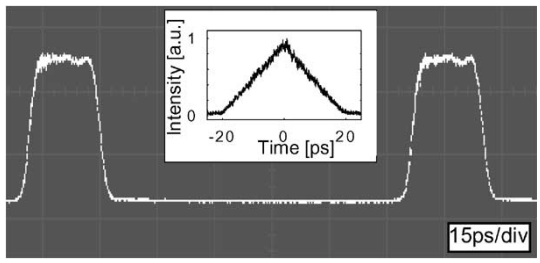

Fig. 5. Optical sampling oscilloscope trace of the 20-ps rectangular pulses. (Inset) Autocorrelation trace of the corresponding rectangular pulses.

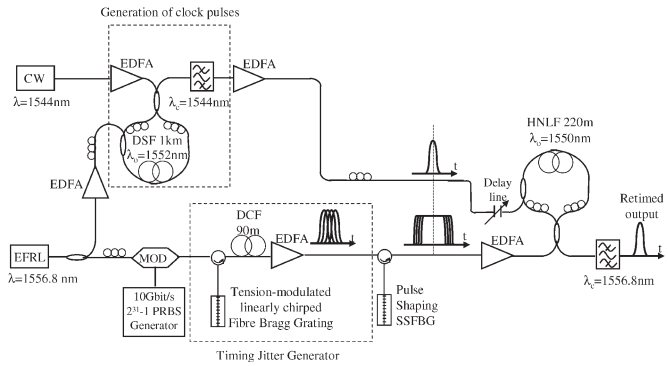

Fig. 6. Experimental setup of the all-optical pulse retiming system using a pulse shaping SSFBG.

features of the pulses can be extracted from this measurement. It, however, confirms that the width of the pulses is $\sim$ 20 ps.

III. Pulse Retiming

The setup we used to implement the optical retiming system is shown in Fig. 6. The pulse source was an actively mode-locked erbium fiber ring laser (EFRL) that was operated at 10 GHz and generated 2.5-ps soliton pulses. The wavelength of operation of the laser was tuned to 1556.8 nm. The pulses were first split using a 50:50 coupler into two separate paths. The first one constituted the data signal. It was modulated by a $2^{31}-1$ pseudorandom bit sequence using a lithium niobate modulator and was then introduced into a timing jitter generator. This consisted of a linearly chirped FBG (with a chirp of 10 ps/nm) with a bandwidth that was broad enough to encompass the full spectrum of the pulses. The FBG was mounted on a stretching rig, which allowed us to periodically modulate the tension applied to the grating with a 500-Hz tone, and thus modulate the physical position from which the pulses were reflected from within the grating. This modulation was in turn translated into a deterministic timing jitter in the reflected signal. The linear chirp acquired by the pulses after their reflection from the FBG was compensated for using a 90-m length of dispersion compensating fiber (DCF) that provided the same magnitude of chirp but of opposite chirp sign. The signal was then fed onto the reshaping SSFBG in order to produce rectangular pulses with a full width of $\sim$ 20 ps. The shaped data pulses were used as the input signal to the retiming NOLM.

The second pulse train component that was split-off from the laser was used for the generation of clean clock pulses at a different wavelength. The pulses were amplified and fed to

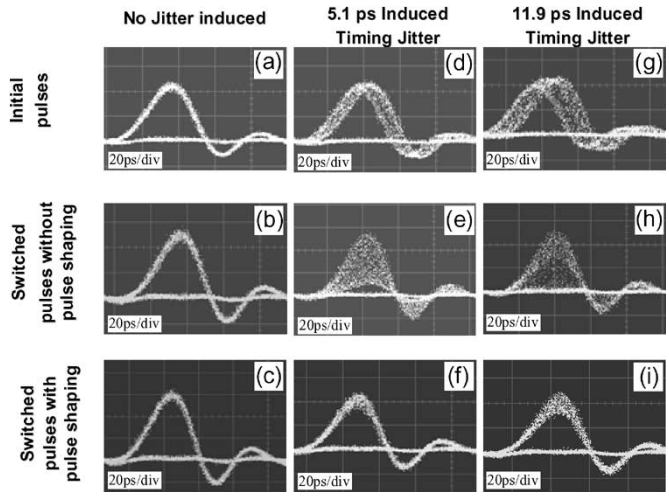

Fig. 7. Eye diagrams at various positions and settings of the system. [Top row: (a), (d), and (g)] At the input to the system and [Bottom row: (c), (f), and (i)] at the output of the system when the retiming technique has been applied. [Middle row: (b), (e), and (h)] At the output of the switch when no reshaping has been applied to the pulses.

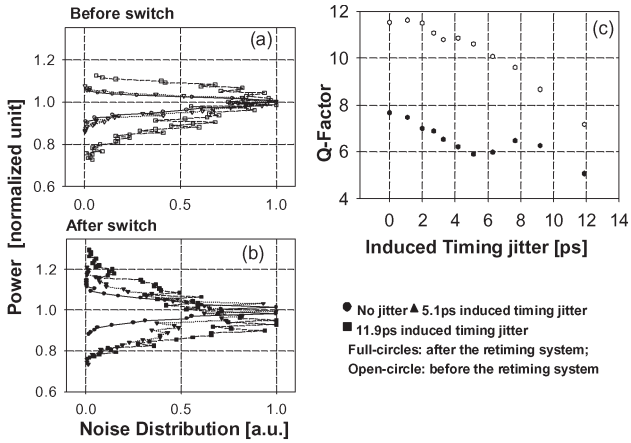

Fig. 8. Noise distributions for three different cases of timing jitter (a) before and (b) after the retiming system. (c) Timing jitter standard deviation versus induced timing jitter characteristic (open circles) before and (full circles) after the retiming system.

the control port of another NOLM, employed as a wavelength converter (WC). The WC-NOLM incorporated a 1-km-long dispersion shifted fiber (DSF) with a zero-dispersion wavelength at 1552 nm. The input signal to this WC-NOLM was a continuous-wave DFB laser operating at 1544 nm. After filtering out the 1556.8-nm control pulses at the loop output, a train of high-quality 2-ps pulses at 1544 nm was generated. These pulses were synchronized to the data stream and were used as the control signal to the second NOLM. The nonlinear element in the retiming NOLM was 220 m of HNLF with a nonlinear coefficient of ~ 20 W^{-1} km^{-1}, a dispersion slope of $+0.030$ ps/nm^2/km, and a zero-dispersion wavelength at 1550 nm.

Since the pulse width of the control pulses is comparable to that of the data pulses, and the walk-off between the two signals inside the NOLM is negligible, the data pulses retain their original pulse width after retiming while maintaining their original wavelength. In order to evaluate the performance of our system, we first examined the retimed signal for the case that no timing jitter was applied to the data pulses. The eye diagrams of Fig. 7(a) and (c) correspond to the data signal at the input and output of the system, respectively, and demonstrate that the retiming system did not in itself introduce significant additional noise to the signal.

We next examined the quality of the output signal for the case when timing jitter was deliberately applied to the incident data pulses. We examined the system performance for several different values of induced timing jitter. We started by adding very little induced timing jitter ($\sim$ 1.1 ps), but gradually increased this up to $\sim$ 11.9 ps, examining system performance on the way. Note that by induced timing jitter we mean the amount of pulse period fluctuation as defined by the amplitude of modulation of the FBG tension. Obviously, the inherent timing jitter of the pulse source itself has to be considered in addition to the induced timing jitter to calculate the corresponding overall timing jitter. Fig. 7(e) and (f) shows an example of eye diagrams at the output of the system when the retiming technique was omitted or included, respectively, for $\sim$ 5.1 ps of induced timing jitter. While the timing jitter manifested itself as severe amplitude noise when the pulse shaper was not included in the system, it was significantly reduced when rectangular pulses were considered. Even in the most extreme case of induced timing jitter that we examined, $\sim$ 11.9 ps, the jitter was eliminated and open eye diagrams were obtained [see Fig. 7(i)], albeit with a slight increase in amplitude noise. We attribute this increase to be in part due to the residual intensity ripple on the top of the rectangular pulses and in part due to some spectral distortion of the signal within the timing jitter generator. In Fig. 8(a) and (b), we present timing jitter distributions for the corresponding three cases of induced timing jitter, before and after the retiming system, respectively. These were obtained from histogram data taken with a digital communications analyzer (DCA) and measured at the full-width at half-maximum (FWHM) point on the leading edge of the pulses. The jitter distributions for the pulses at the input of the system show a double peaked feature as expected from the sinusoidal modulation of the tension applied on the chirped grating. Fig. 8(b) shows the timing jitter distribution of the retimed pulses. In both cases, the final timing jitter distribution approaches that measured for the seed laser.

Fig. 8(c) shows the standard deviation of the timing jitter both before and after the retiming system as a function of the induced timing jitter. The jitter of the pulses after the retiming system remained fairly constant for all values of induced timing jitter. Note that the level of $\sim$ 1 ps of root mean square timing jitter corresponds to the noise limit of the DCA used for our measurements.

Histogram data on the pulse amplitude noise (as measured at the pulse center) were also examined for the retimed pulses for the same three cases shown in Fig. 7 and the corresponding distributions are plotted in Fig. 9(a) and (b). For the unjittered case, the amplitude noise of the retimed pulses was similar to that of the initial pulses; however, as induced timing jitter is applied, increased amplitude noise is observed, as previously discussed. Fig. 9(c) shows the corresponding Q-factor values of the eye diagrams as a function of induced timing jitter. A

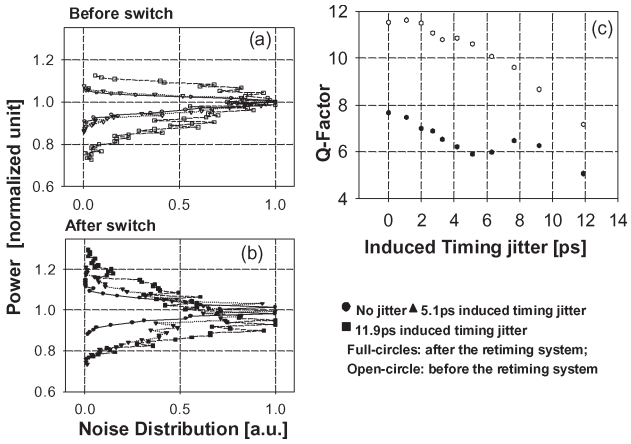

Fig. 9. Noise distributions for three different cases of amplitude jitter (a) before and (b) after the retiming system. (c) Q-factor versus induced timing jitter characteristic (open circles) before and (full circles) after the retiming system.

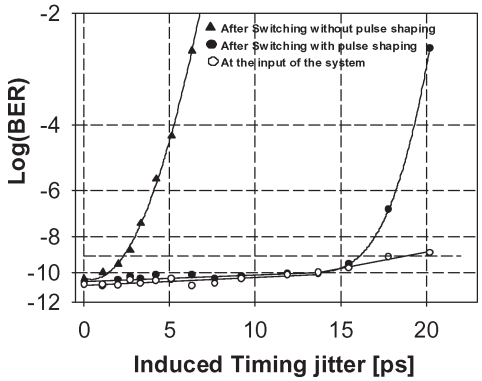

Fig. 10. BER measurements versus induced timing jitter characteristic (open circles) before and after the switch (full triangle) without and (full circles) with pulse shaping for a constant received optical power of -21 dBm.

degradation of the Q-factor even before the retiming system is noticeable from the curve, which can be attributed to the "mark level" appearing thicker at the pulse center due to the added timing jitter. The corresponding Q-factor curve for the pulses after the retiming system shows some degradation in the signal in terms of amplitude noise, even though all the Q-values are around 6, which would correspond to error-free operation of the system under normal noise distribution conditions. In order to confirm this, we carried out BER measurements for various values of induced timing jitter. The measurements were taken for a constant input power of -21 dBm at the receiver and are summarized in Fig. 10. The performance of the system after the retiming stage is compared to that when no pulse shaping is applied and when no retiming is applied at all. It has to be appreciated, however, that the degradation of the quality of the optical signal due to the introduction of timing jitter does not have a significant effect on the measured BER performance due to the lowpass filtering within the 10-GHz receiver used for our BER measurements, which makes it insensitive to jitter of the order of a few picoseconds. Nevertheless, Fig. 10 shows a clear improvement in the performance of the switch when pulse shaping was applied relative to the case when the SSFBG was not included into the system. With the grating in place, error-free operation was only possible if the timing jitter was less than the duration of the rectangular pulses. When the induced timing jitter exceeded the width of the rectangular pulses, the noise behavior of the system became similar to that when no reshaping was applied.

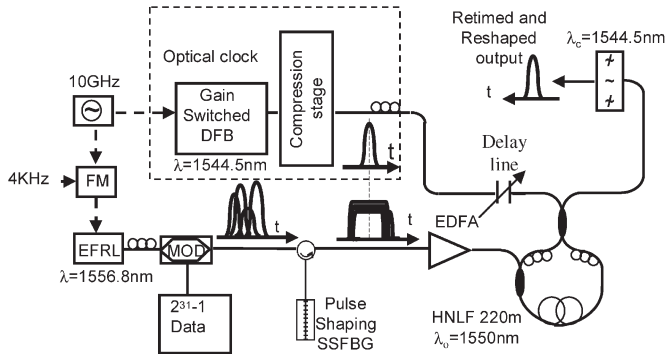

Fig. 11. Experimental setup of the simultaneous retiming–reshaping system.

Although the results we achieved were excellent in terms of eliminating timing jitter itself, the fact that the Q-values of the eye diagrams degraded after the switch indicates that an amplitude regeneration stage should also ideally be incorporated within the system. The performance of the system with an amplitude regenerator included is discussed in the following section.

IV. Pulse Reshaping and Retiming

Although the previous configuration had the benefit of maintaining the wavelength of the data signal while drastically reducing the timing jitter, the fact that it does not provide any amplitude regeneration may limit its practical application. In this section, we present a modification to the previous setup that makes use of the regenerative properties of the NOLM configuration in order to obtain reshaping/amplitude noise reduction as well as retiming of the data pulses.

The new experimental setup is shown in Fig. 11. In this case, two independent and synchronized laser sources operating at two different wavelengths, one for the clock and the other for the data signal, were employed. The data source was again a 10-GHz actively mode-locked EFRL generating 2.5-ps soliton pulses at the operating wavelength of 1556.8 nm, and was externally modulated with a $2^{31}-1$ pseudorandom data sequence using a lithium niobate modulator. Timing jitter in this instance was directly introduced to the laser source by frequency modulating the mode-locking RF drive signal to the EFRL with a 4-kHz tone, obtaining similar timing jitter performance compared to the previous grating-based configuration. The amount of induced timing jitter could be varied by varying the amplitude of the frequency modulation applied to the 10-GHz drive signal. In addition to this, we degraded the extinction ratio between the marks and spaces of the data by choosing a nonoptimum bias voltage for the operation of the lithium niobate data modulator. This allowed us to degrade the Q-factor of the data pulses from 17.5 to 7.4. The pulses were then fed onto the pulse-shaping SSFBG to convert the 2.5-ps solitons into 20-ps rectangular pulses. In contrast to the previous case, the shaped data pulses were now used as the (high

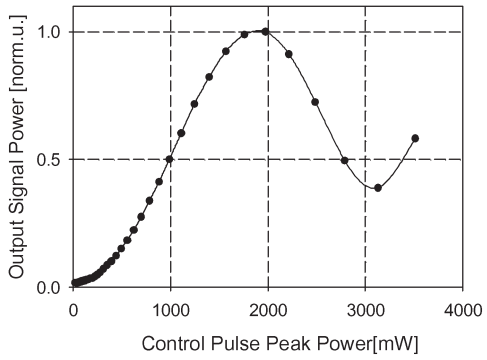

Fig. 12. Nonlinear transfer characteristic of the NOLM.

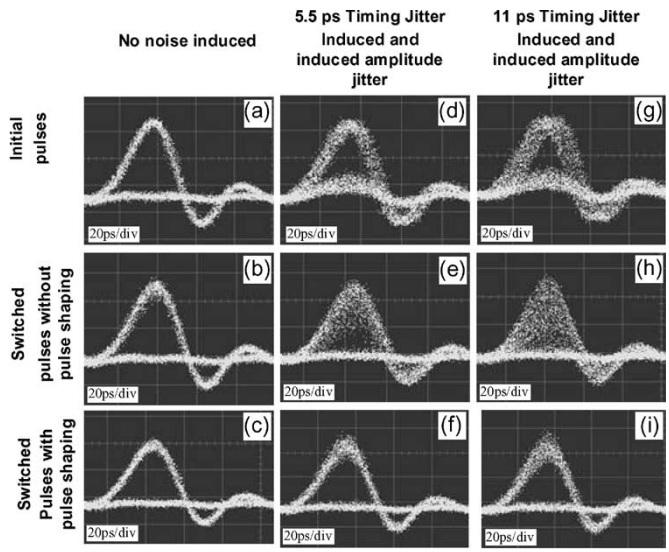

Fig. 13. Eye diagrams at various positions and settings of the system. [Top row: (a), (d), and (g)] At the input to the system and [Bottom row: (c), (f), and (i)] at the output of the system when the retiming technique has been applied. [Middle row: (b), (e), and (h)] At the output of the switch when no reshaping has been applied to the pulses.

power) control signal to the NOLM switch. The measured transfer characteristic of the NOLM used is shown in Fig. 12. The shaped data signal was amplified, using a commercial erbium-doped fiber amplifier (EDFA), to a sufficient power level to ensure that the operating point of the NOLM reached the flat region of the transfer characteristic—corresponding to $\sim$ 2 W of peak power. The input signal to the NOLM was provided by a gain-switched DFB laser that operated at 1544.5 nm and was driven by a 10-GHz RF signal synchronized to the mode-locked fiber laser oscillator. The pulses of the gain-switched DFB laser were compressed down to $\sim$ 2 ps using a 125-m length of DCF followed by a nonlinear compression stage comprising of an EDFA and 490 m of an HNLF. In order to evaluate the performance of our system, we repeated similar measurements to those previously made on the configuration of Section III. The system performance was assessed for the case when timing jitter was added together with amplitude noise onto the data. For our measurements, we applied a constant amount of amplitude noise and took data for five different values of induced timing jitter ranging from $\sim$ 0.8 to $\sim$ 11 ps, which represents an extreme value of induced timing jitter and

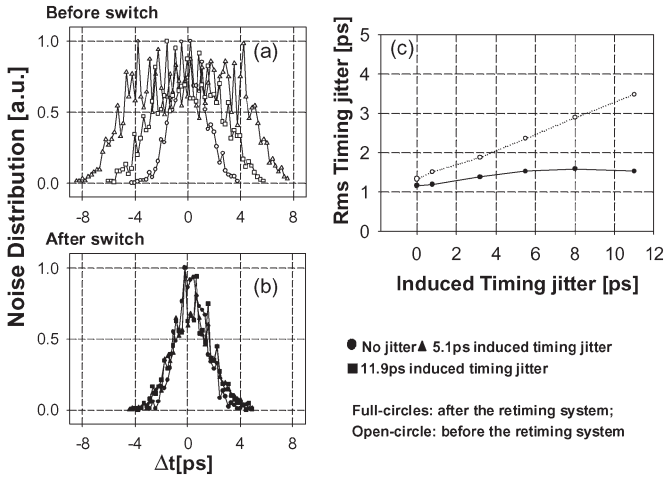

Fig. 14. Distributions for three different cases of timing jitter (a) before and (b) after the retiming system. (c) Timing jitter standard deviations versus induced timing jitter characteristic (open circle) before and (full circle) after our system.

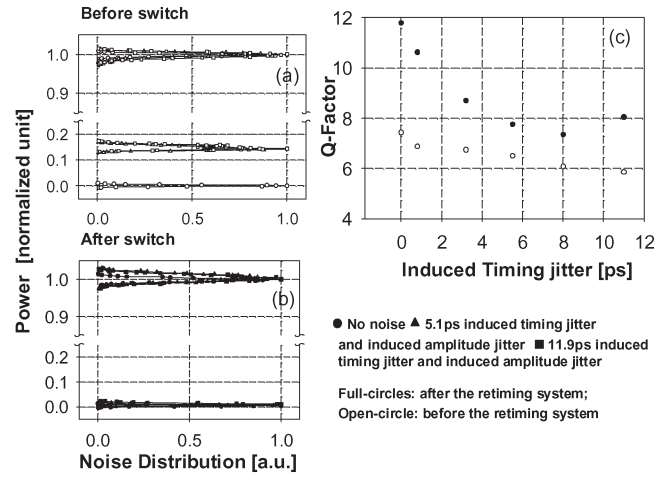

Fig. 15. Distributions for three different cases of amplitude jitter (a) before and (b) after the retiming system. (c) Q-factor values versus induced timing jitter (open circle) before and (full circle) after our system.

a significant test of our system. Eye diagrams for three different induced timing jitter settings of the system are shown in Fig. 13. Fig. 13(a) and (c) corresponds to the data signal at the input and the output of the system, respectively, for the case when no noise is induced, demonstrating that the retiming and reshaping system does not in itself introduce any additional noise to the signal. Fig. 13(d)–(i) demonstrates that after the inclusion of the pulse shaping SSFBG, the timing jitter is eliminated at the output of the system and open eyes are obtained for both cases of induced timing jitter. When pulse shaping is not applied, there is severe degradation in the quality of the eye diagrams [Fig. 13(e) and (h)], which is evident even for relatively small values of timing jitter. To illustrate this point more clearly, we performed histogram analysis on the eye diagrams. The results are summarized in Figs. 14 and 15. In Fig. 14(a) and (b), we present timing jitter distributions for the three cases considered in Fig. 13 before and after the system. A graph of the standard deviation of the timing jitter before and after the system as a function of the induced timing jitter is shown in Fig. 14(c).

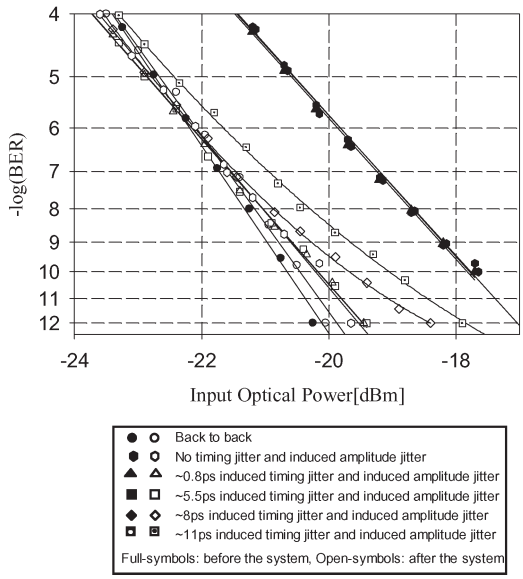

Fig. 16. BER curves at various positions and settings of the system.

As expected from the previous discussion in Fig. 8, the pulses at the output of the switch are retimed and the timing jitter for all cases approaches the resolution limit of our DCA. The intensity histograms of Fig. 15 demonstrate that the amplitude noise associated with the "zero bits" is drastically reduced, as intuitively suggested by the flat region of the nonlinear transfer characteristic for low-input power values (see Fig. 12). The amplitude noise on the marks remains roughly constant for low values of induced timing jitter owing to the reshaping capabilities of this NOLM configuration, in contrast to the previous configuration described in Section III. However, on increasing the induced timing jitter, some additional amplitude noise appears on the marks, which could be attributed to slight distortions of the rectangular pulses close to their edge resulting from self-phase modulation experienced by the data signal during propagation in the HNLF. Fig. 15(c) shows Q-factor values for all the cases both before and after the system. An improvement in the Q-factor from 7 to 11 was achieved in the instance that ~ 0.8 ps of timing jitter is induced in the system. In the worst condition of ~ 11 ps of induced timing jitter, an improvement from 5.9 to 8 was measured. BER measurements of the system are presented in Fig. 16. We first characterized the system for the case when no noise was added, and confirmed that there was no power penalty relative to the back-to-back case. We next considered the case where only amplitude noise was deliberately applied to the incident data pulses. An improvement in the receiver sensitivity of more than 2.3 dB was achieved after the switch, demonstrating the amplitude noise reduction provided by the NOLM. Once again, it is worth noting that the BER curves of the input signal are insensitive to timing jitter due to the low-pass action of the electronic receiver. Hence, for the same amplitude noise setting, the BER curves of the input signal overlapped for all cases of induced timing jitter that we examined. As long as the induced timing jitter values remained lower than ~ 5.5 ps, the BER curves at the output of the reshaping–retiming system still overlapped with the back-to-back curve. For more extreme cases, a small power penalty in the BER curves (~ 1 dB for ~ 11 ps of induced timing jitter) was observed, as previously discussed. Nevertheless, for all cases, there was a clear improvement in the BER performance of the signal after the introduction of the reshaping–retiming system.

V. Conclusion

In this paper, we have demonstrated a powerful technique for the retiming and reshaping of short optical pulses. The technique relies on linear pulse shaping of the data pulses into rectangular pulses, performed using an SSFBG, and subsequent optical switching with synchronous optical clock pulses. The amount of timing jitter that can be compensated for is determined by the width of the rectangular pulses and can be readily adjusted to fit the specific jitter characteristic of a given transmission system. It has already been demonstrated that SSFBG technology is suitable for generating temporal features as short as 3.1 ps [11], a number that by no means represents the ultimate limit of the technology. The combination of rectangular pulses with such a short pulse width with nonlinear optical switches that exploit the ultrafast Kerr effect in optical fibers (femtosecond response times) should allow the regeneration of signals with bit rates as high as 320 Gb/s. In order to fully analyze the performance of our scheme, we considered two different configurations. In the first one, the shaped data formed the low-power signal to the NOLM switch in order to perform pure retiming of the signal. While this allowed us to maintain the wavelength of the data signal after switching, it made the performance of the system susceptible to any amplitude noise of the original data as well as to nonuniformities of the nominally flat section of the rectangular-shaped pulses. By feeding the shaped signal into the control port of the NOLM in the second configuration, we were able to overcome these issues and perform reshaping of the signal as well as retiming. In this paper, we have demonstrated the operating principle of the technique at 10 Gb/s. We plan to apply the approach in transmission experiments at higher repetition rates in the near future.

References

[1] B. J. Eggleton, P. A. Krug, L. Poladian, and F. Ouellette, "Long periodic superstructure Bragg gratings in optical fibres," *Electron. Lett.*, vol. 30, no. 19, pp. 1620–1622, Sep. 1994.

[2] P. C. Teh, P. Petropoulos, M. Ibsen, and D. J. Richardson, "A comparative study of the performance of seven- and 63-chip optical code-division multiple-access encoders and decoders based on superstructured fiber Bragg gratings," *J. Lightw. Technol.*, vol. 19, no. 9, pp. 1352–11365, Sep. 2001.

[3] P. Petropoulos, M. Ibsen, M. N. Zervas, and D. J. Richardson, "Generation of a 40-GHz pulse stream by pulse multiplication with a sampled fiber Bragg grating," *Opt. Lett.*, vol. 25, no. 8, pp. 521–523, Apr. 2000.

[4] P. Petropoulos, M. Ibsen, A. D. Ellis, and D. J. Richardson, "Rectangular pulse generation based on pulse reshaping using superstructured fiber Bragg grating," *J. Lightw. Technol.*, vol. 19, no. 5, pp. 746–752, May 2001.

[5] J. H. Lee, L. K. Oxenløwe, M. Ibsen, K. S. Berg, A. T. Clausen, D. J. Richardson, and P. Jeppesen, "Timing jitter tolerant all-optical TDM data demultiplexing at 80 Gb/s using fiber Bragg grating based rectangular pulse switching technology," in *Proc. Optical Fiber Communications Conf. (OFC)*, Atlanta, GA, 2003, pp. 200–201.

[6] K. Uchiyama, T. Morioka, S. Kawanishi, H. Takara, and M. Saruwatari, "Signal-to-noise ratio analysis of 100 Gb/s demultiplexing using nonlinear optical loop mirror," *J. Lightw. Technol.*, vol. 15, no. 2, pp. 194–201, Feb. 1997.

[7] J. H. Lee, P. C. Teh, P. Petropoulos, M. Ibsen, and D. J. Richardson, "Timing jitter tolerant all-optical modulator and demultiplexing systems incorporating pulse-shaping fiber Bragg gratings," in *Proc. Optical Fiber Communications Conf. (OFC)*, Anaheim, CA, 2001, pp. PD30-1–PD30-3.
[8] C. Schubert, R. Ludwig, S. Watanabe, F. Futami, S. Ferber, J. Berger, C. Schmidt, and H. G. Weber, "Improved performance of a 160 Gb/s fibre based all-optical switch using rectangular gating pulses," presented at the Proc. Eur. Conf. Optical Communication (ECOC), Copenhagen, Denmark, 2002, Paper 8.3.7.
[9] N. J. Doran and D. Wood, "Nonlinear-optical loop mirror," *Opt. Lett.*, vol. 13, no. 1, pp. 56–58, Jan. 1988.
[10] F. Parmigiani, P. Petropoulos, P. J. Almeida, M. Ibsen, J. H. Lee, and D. J. Richardson, "A direct assessment of the performance of pulse shaping superstructured fiber gratings using an optical sampling oscilloscope," in *Proc. Optical Fiber Communications Conf. (OFC)*, Atlanta, GA, 2003, pp. 40–42.
[11] P. C. Teh, M. Ibsen, J. H. Lee, P. Petropoulos, and D. J. Richardson, "Demonstration of a four-channel WDM/OCDMA system using 255-chirp, 320 Gchip/s quaternary phase coding gratings," *IEEE Photon. Technol. Lett.*, vol. 14, no. 2, pp. 227–229, Feb. 2002.

Francesca Parmigiani was born in Milan, Italy. She graduated with a degree in electronic engineering at Politecnico di Milano, Milano, Italy, in 2002, and is currently working toward the Ph.D. degree in optical communication systems at the Optoelectronics Research Centre, University of Southampton, Southampton, U.K.

Her research interests include optical sampling technique, pulse shaping, and nonlinear processing to perform all-optical regeneration.

Ms. Parmigiani is a member of the Optical Society of America (OSA).

Periklis Petropoulos was born in Patras, Greece. He graduated from the Department of Electrical Engineering and Information Technology, University of Patras, in 1995, received the M.Sc. degree in communications engineering from the University of Manchester Institute of Science and Technology, Manchester, U.K., in 1996, and the Ph.D. degree in optical telecommunications from the Optoelectronics Research Centre (ORC), University of Southampton, Southampton, U.K. in 2000.

His research interests include all-optical processing and switching in optical fibers; pulse manipulation for optical communications using fiber Bragg gratings, including applications in optical correlation systems for the implementation of optical code division multiple access and optical packet switched systems; silica and compound glass holey fibers and their nonlinear applications; and fiber lasers. His research has produced more than 100 papers in journals and conferences in the field of optical physics and optical communications. He is currently a Southampton Senior Research Fellow at the ORC.

Morten Ibsen was born in Copenhagen, Denmark. He graduated with degrees in physics, mathematics, and optical communications at the IFA-University of Aarhus, Denmark, OFTC-University of Sydney, Australia, and Optoelectronics Research Centre (ORC)-University of Southampton, Southampton, U.K., respectively.

His current interests include specialized Bragg grating design, fabrication, and characterization; and dynamic aspects of Bragg gratings including pulse shaping and tunable dispersion equalization together with devices and systems utilizing Bragg gratings. These include single-frequency DFB fiber lasers and complex code generators in optical code-division multiple-access (OCDMA) applications. Furthermore, recently he has started work on the exploitation of Bragg grating technology in medicine, therapeutic health applications, and imaging.

Dr. Ibsen is a member of the Optical Society of America (OSA). He currently holds a Royal Society of London, University Research Fellowship (URF).

David J. Richardson was born in Southampton, U.K., in 1964. He received the B.Sc. degree and the Ph.D. degree in fundamental physics from Sussex University, U.K., in 1985 and 1989, respectively.

In May 1989, he was a Research Fellow at the then recently formed Optoelectronics Research Centre (ORC), Southampton University, U.K. He is currently a Deputy Director at the ORC, responsible for much of the ORC's fiber-related activities. He is one of the founders of Southampton Photonics Incorporated, a university spin-off venture that has successfully commercialized elements of high-power laser technology developed within the ORC. His current research interests include amongst others: holey fibers, high-power fiber lasers, short pulse lasers, optical fiber communications, all-optical processing and switching, nonlinear optics, and the physics and applications of microstructured nonlinear/linear media. He has published more than 400 conference and journal papers in his 15 years at the ORC and produced over 15 patents.

Prof. Richardson is a frequent Invited Speaker at leading international optics conferences in the optical communications, laser, and nonlinear optics fields, and an active member of both the national and international optics communities. He was awarded a Royal Society University Fellowship in 1991 in recognition of his pioneering work on short-pulsed fiber lasers.